Society of Economic Geologists
Special Publication 10, 2003, p. 41–59

Chapter 3

Melt Inclusion Study of the Embryonic Porphyry Copper System at White Island, New Zealand

M. H. RAPIEN, R. J. BODNAR†

Department of Geological Sciences, Virginia Polytechnic Institute and Stage University, Blacksburg, Virginia 24061-0420

S. F. SIMMONS,

Geothermal Institute, University of Auckland, Private Bag 92019, Auckland, New Zealand

C. S. SZABO,

Department of Petrology and Geochemistry, Institute of Geology, Eotvos University, Budapest, Hungary H-1088

C. P. WOOD,

Institute of Geological and Nuclear Research, Wairakei Research Center, Private Bag 2000, Taupo, New Zealand

AND S. R. SUTTON

Department of Geophysical Sciences and Center for Advanced Radiation Sources, University of Chicago, Chicago, Illinois 60637

Abstract

White Island, New Zealand, is an active andesitic-dacitic volcano that is located near the southern end of the Tonga-Kermadec-Taupo Volcanic Arc at the convergent plate boundary where the Pacific plate is being subducted beneath the Indian-Australian plate. The plate tectonic setting, volcanic features, and petrology of White Island are characteristic of the environment associated with formation of porphyry copper deposits. White Island has been active for at least 10 ka and, as such, is an ideal location to study early magmatic processes associated with formation of porphyry copper deposits. In this study, the geochemistry of the magma chamber at White Island has been characterized through analyses of silicate melt inclusions, phenocrysts, and matrix glass contained in recent ejecta (1977–1991). Most melt inclusions in samples from the 1977, 1988, and 1989 eruptions contained only glass and occasional vapor bubbles and/or trapped solids. The 1991 sample contained daughter minerals, suggesting a different P-T history compared to the other samples.

Data obtained from White Island are compared to various major, trace element, and volatile composition trends reported for both economic and noneconomic (or barren) porphyry deposits. Magmas associated with economic porphyry copper deposits are generally peraluminous with $Al_2O_3/(Na_2O + K_2O + CaO)$ ratios greater than or equal to 1.3, and compositions of melt inclusions from White Island equal or exceed this value. Glass in unhomogenized 1991 melt inclusions is corundum normative, with $Si/(Si + Ca + Mg + Fe_{total}) > 0.91$, and $K/(K + Ca + Mg + Fe_{total}) > 0.36$. Melt inclusions from White Island show a positive Eu anomaly. All of these features are characteristic of productive systems. Trends in high field strength elements versus Y and in Mn versus Y are more consistent with barren intrusions than with productive plutons.

Analyses of five melt inclusions from White Island indicate Cu concentrations sufficiently high (up to several hundred ppm) to generate an economic porphyry copper deposit, based on theoretical models. Moreover, high Cl/H_2O ratios (0.15) in melt inclusions favor the efficient extraction of copper from melt by the magmatic aqueous phase. Mineral phases, such as pyrrhotite, biotite, or amphibole, which might scavenge copper from the melt before it could be partitioned into the magmatic vapor phase, are absent. Concentrations of S in the melt are low, which further inhibits pyrrhotite crystallization. The oxidation state of the magma at depth, based on the presence of SO_2 in the magmatic gas, is consistent with that predicted for porphyry copper magmas.

Combined geochronologic, tectonic, petrologic, and geochemical data suggest that White Island may represent an embryonic porphyry copper system that has not yet reached the productive stages of copper mineralization.

†Corresponding author: e-mail, rjb@vt.edu

Introduction

FOR NEARLY a century, starting with the classic work of Lindgren (1905) and continuing to the present (Sales, 1954; Stringham, 1960; Titley and Beane, 1981; Lang and Titley, 1998), workers have attempted to characterize magmatic systems associated with the formation of porphyry copper deposits. Although much has been learned during the past 100 yr, our understanding of the earliest magmatic stage of porphyry copper formation is still incomplete, owing to the often wholesale destruction of early magmatic phases by later magmatic and hydrothermal events. In this study we have attempted to minimize the problem of later overprinting and destruction of early magmatic phases by studying an active system that may be in the embryonic stages of porphyry copper formation.

White Island is an active andesitic-dacitic volcano located near the southern end of the Tonga-Kermadec-Taupo Volcanic Arc, at the convergent plate boundary where the Pacific plate is being subducted beneath the Indian-Australian plate (Cole and Lewis, 1981). White Island is located about 200 km west of the Kermadec trench, where magmas are generated from the gently dipping subducted oceanic plate that lies about 80 to 100 km beneath the island (Cole and Lewis, 1981). It is now generally accepted that porphyry copper deposits form at convergent plate boundaries where magmas generated from a subducting slab and/or mantle wedge migrate upward to produce shallow silicic plutons (Sillitoe, 1972; Sawkins, 1984). The tectonic setting of White Island is thus similar to that associated with the formation of porphyry copper deposits elsewhere.

The modern magmatic-hydrothermal system at White Island is evidenced by surface features that include high-temperature fumaroles and acid springs. For over two decades since 1970, these features were the sites of detailed monitoring and fluid sampling by Werner Giggenbach, making it one of the best studied, if not best understood, systems in the world (Giggenbach, 1987; Giggenbach and Sheppard, 1989; Giggenbach et al., 2003). Hedenquist et al. (1993) and Hedenquist and Lowenstern (1994) noted that the near-surface geochemical environment at White Island is similar to that envisioned for the formation of high-sulfidation Cu-Au mineralization at other locations. Furthermore, Sillitoe (1983, 1995) reported compelling evidence for a direct genetic link between high-sulfidation epithermal deposits and porphyry copper mineralization in many systems in the circum-Pacific and Alpine-Himalayan belts, and Bodnar and Beane (1980) described enargite-type mineralization underlain by subeconomic porphyry copper-type mineralization at Red Mountain, Arizona. More recently, Arribas et al. (1995) and Hedenquist et al. (1998) documented a clear genetic link between near-surface, high-sulfidation Cu-Au mineralization and deeper porphyry-type mineralization in the Lepanto-Far Southeast Cu-Au deposit in the Philippines. There is thus a well-defined worldwide link between shallow epithermal enargite-type mineralization and deeper porphyry copper-type mineralization.

At White Island, copper is currently being released into the atmosphere at an estimated rate of 300 kg/d during continuous degassing of the volcano (Rose et al., 1986; Tedesco and Toutain, 1991; Le Cloarec et al., 1992). Near-surface acid brines, produced when acid gases mix with ground water, are depleted in copper. Giggenbach (1987) suggested that the low copper values may be explained by deposition of a Cu-rich mineral, such as enargite, in the subsurface. Based on these observations, it is logical to suggest that White Island represents a modern ore-forming system in which epithermal high-sulfidation Cu-Au mineralization is forming in the near-subsurface and overlies an environment conducive to the formation of deeper porphyry copper-type mineralization.

Although there have been numerous geochemical and fluid inclusion studies of porphyry copper deposits (Roedder and Bodnar, 1997), conditions during the early magmatic stage have been difficult to characterize because early magmatic assemblages are commonly overprinted by later magmatic and hydrothermal events (Beane and Titley, 1981; Beane, 1982; Beane and Bodnar, 1995; Student, 2002). The magmatic-hydrothermal system at White Island, however, is still in its infancy relative to the porphyry copper mineralization stage and thus provides an opportunity to document the early history of a potential porphyry copper-forming system. Moreover, melt inclusions within ejecta provide a sample of melt that was trapped in the magma chamber at some depth beneath White Island. As such, the melt inclusions record the volatile and metal concentrations of the silicic melt at depth, at a time (presumably) before the major episodes of copper mineralization have occurred. In this study, phenocrysts, silicate melt inclusions, and matrix glass contained in ejecta from White Island were examined. Major, trace element, and volatile concentrations of melt inclusions and matrix glass were determined to characterize the early magmatic system at White Island, and these data have been compared to results from other economic as well as barren porphyry systems.

Geologic Setting

The North Island of New Zealand (Fig. 1) is located above an active plate boundary where the Pacific plate is being subducted beneath the eastern margin of the Indian-Australian plate (Isacks et al., 1968; Cole and Lewis, 1981), producing an active zone of intermediate to deep earthquakes and associated volcanism (Dickinson and Hatherton, 1967; Hamilton and Gale, 1968). The North Island has four compositionally distinct zones of volcanic activity, including the Bay of Islands, Auckland, Egmont, and the Taupo Volcanic Zone (Fig. 1). The Taupo Volcanic Zone is located 200 to 270 km west of the Kermadec-Hikurangi trench and extends 250 km from the central North Island northeast to White Island (Fig. 1). Volcanoes in the Taupo Volcanic Zone range from basaltic to rhyolitic in composition, with White Island being andesitic to dacitic in composition (Cole and Nairn, 1975).

White Island is the summit of a large submarine volcanic massif that measures 16 by 18 km at its base, which rests on

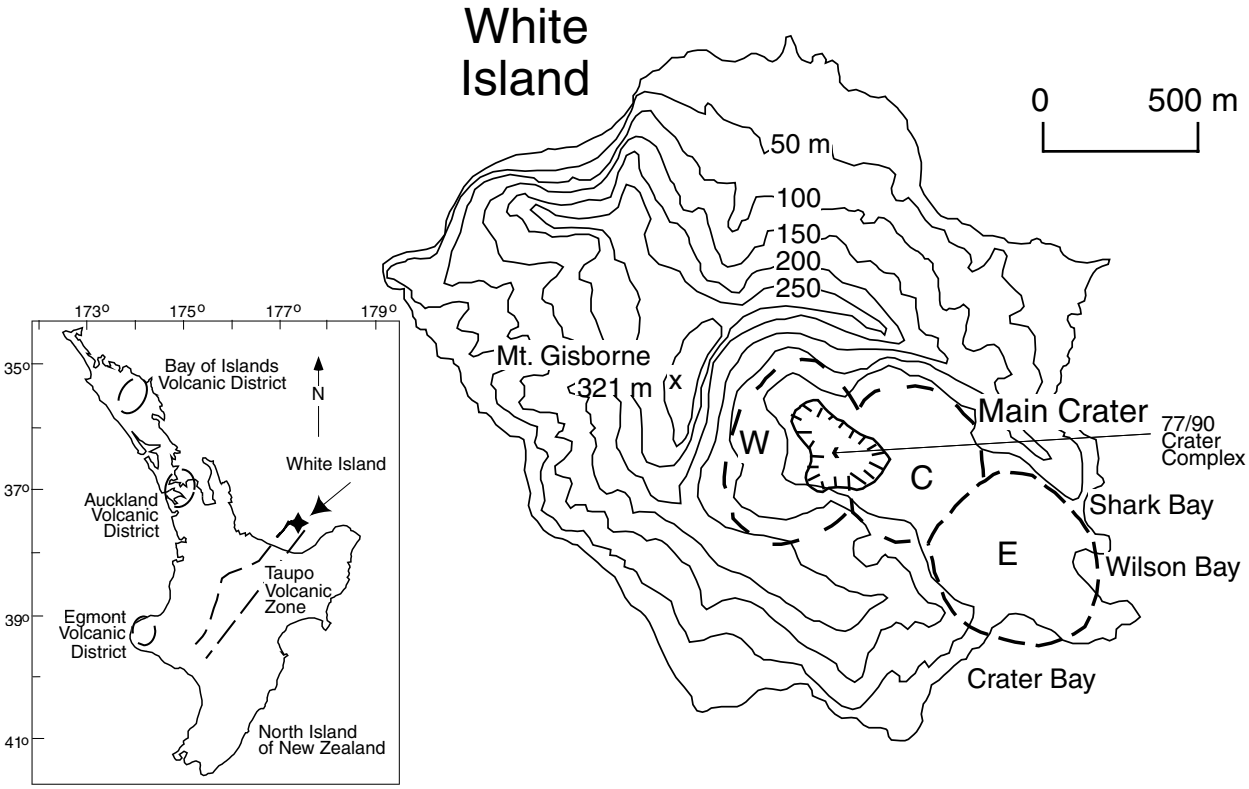

FIG. 1. Location map of White Island showing the main topographic features. W, C, and E show locations of the western, central, and eastern subcraters, respectively.

the sea floor at 300- to 400-m water depth. The volcano is a 700-m-high composite volcano consisting of two overlapping cones, with the western part being older than the central and eastern parts (Black, 1970). The island reaches a height of approximately 320 m above sea level and extends 2.4 km in the east-west direction and 2 km in the north-south direction. Erosion on wave-cut cliffs and gullies on the outer part of the cone indicate that long periods of quiescence interrupted cone building episodes at White Island (Cole and Nairn, 1975).

One of the most notable topographic features of White Island is the breached main crater. In 1914, a collapse occurred along a fault in the southwestern rim of the breached crater, killing several sulfur mine workers (Cole and Nairn, 1975). The main crater is 1.25 km long and 0.5 km wide, and consists of three subcraters: eastern, central, and western (Fig. 1). Recent volcanic activity has occurred in the western subcrater and in the western part of the central subcrater (Houghton and Nairn, 1991).

Recent Volcanic Activity

White Island has been in a state of continuous fumarolic activity, with intermittent steam and tephra eruptions, since the first Europeans landed on the island in 1826 (Cole and Nairn, 1975). White Island was discovered and named by James Cook over 50 yr earlier (1769), but Cook made no mention of volcanic activity (Clark and Cole, 1989). However, volcanic activity previous to Cook's discovery is evidenced by the frequent mention of White Island in Maori legends (Cole and Nairn, 1975). The historic activity is similar to recent eruption patterns with crater-forming eruptions occurring in 1933, 1947, 1965 to 1966, 1968, 1971, 1976 to 1982, and 1986 to 1992 (Houghton and Nairn, 1991; Wood and Browne, 1996). Estimates from trace metal enrichment of marine sediments suggest that the volcano and its associated hydrothermal system have been active for the past 10,000 yr (Giggenbach and Glasby, 1977).

In mid-1973 a large (approximately 10^6 m^3) body of basaltic andesite magma began to rise to a shallow emplacement depth (0.5 km) at White Island and continued to rise until eruptive activity started in 1976 (Clark and Cole, 1989). Intense volcanic activity continued over the next several years, consisting of alternating strombolian and phreatomagmatic eruptions. The volcano continuously erupted for about 16 yr, allowing effective release of magmatic gases. Exsolved gases interacted with the surrounding hydrothermal system, acidifying the hydrothermal fluids.The acidified fluids permeated the crater floors and altered the rocks, weakening substructures and making them susceptible to collapse during later earthquake activity (Houghton and Nairn, 1989a, 1991). The condition of the crater floors and conduit system, in turn, influenced the eruptive style at White Island. That is, continuous phreatomagmatic events erupting mainly ash occurred

when conduit walls were stable. Discrete explosions, producing juvenile block aprons, occurred when conduit walls were weakened and/or clogged (Houghton and Nairn, 1989a, 1991).

A second sequence of eruptive activity at White Island began in February, 1986, with a discrete phreatomagmatic eruption. Volcanic activity during this eruption period consisted of continuous gas emissions, interrupted by frequent alternating strombolian and phreatomagmatic eruptions. This eruptive activity continued until May 1992 (Wood and Browne, 1996).

Representative samples of ejecta from seven eruptions that occurred between 1977 and 1991 were used in this study. After preliminary examination of all samples, those from the 1977, 1988, 1989, and 1991 eruptions were chosen for study, owing to their abundance of silicate melt inclusions.

Analytical Techniques

Samples were examined both in hand specimen and in doubly polished thin sections, using transmitted and reflected light microscopy. Plagioclase phenocrysts were etched with fluoboric acid and examined using differential interference contrast microscopy (Anderson, 1983) to highlight chemical zoning that might not be obvious with standard petrographic techniques. Major element compositions of phenocrysts, silicate melt, and mineral inclusions in phenocrysts, and matrix glass were determined by electron microprobe. In addition, copper and zinc concentrations of five melt inclusions, as well as matrix glass and phenocrysts contained in the 1977 sample, were determined by electron microprobe and synchrotron XRF analyses. Trace element and volatile contents of melt inclusions and matrix glasses from the 1988 and 1989 samples were measured by ion microprobe. Multiphase silicate melt inclusions (containing daughter minerals) hosted in orthopyroxene from the 1991 sample were heated to homogenize the inclusions. The major element chemistry of glass in the homogenized inclusions was determined by electron microprobe.

Major element and copper and zinc concentrations were determined using a Cameca SX50 electron microprobe, equipped with both wave and energy dispersive spectrometers (WDS and EDS, respectively). Quantitative analyses were conducted using WDS. Backscattered electron imaging was used to distinguish between silicate melt and mineral inclusions, as well as to test for the presence of microlites in areas of matrix glass selected for analysis. Natural and synthetic silicate and oxide standards were used as appropriate, and data were corrected using Pouchou and Pichoir (PAP) methodology according to Pouchou and Pichoir (1985). Analyses were performed at 15 kV, with a beam current of 10 nA and a 5 μm beam size, except for Cu and Zn, which used 35kV and 50 nA. Although Na was analyzed first, there was likely some Na loss owing to the relatively high beam currents used (Morgan and London, 1996)

Ion microprobe analyses were performed on a Cameca IMS-6F ion microprobe equipped with both oxygen and cesium guns at the Department of Terrestrial Magnetism at the Carnegie Institution of Washington. Trace elements were analyzed in situ using a 12.7 kV primary beam of O^- ions with a current of 0.5 to 2 nA focused to a diameter of 10 to 20 μm. Positively charged secondary ions were analyzed at a nominal accelerating voltage of +10 kV. The secondary ion beam was energy filtered using an energy offset of –70 eV and an energy window of ±25eV. Secondary ions were counted by an electron multiplier, manufactured by ETP Ltd., that feeds into an emitter-coupled logic (ECL) counting system with a deadtime of 13 ns. Secondary ion counts were referenced to counts for ^{30}Si (e.g. $^{90}Zr/^{30}Si$, $^{93}Nb/^{30}Si$) and absolute abundances of trace elements were calculated from standard calibration curves developed at the Department of Terrestrial Magnetism. The scatter of standards about the calibration curves was generally less than 10 percent, similar to the reproducibility of individual analyses on homogeneous standards. Thus, analytical uncertainty on individual analyses is typically ±10 percent except where low numbers of ions indicate a larger standard deviation.

Volatile elements (H, S, and Cl) were analyzed in situ using a 10 kV primary beam of Cs+ ions with a current of 3 to 8 nA focused to a diameter of 20 to 30 μm. Negatively charged secondary ions were analyzed at a nominal accelerating voltage of +5 kV. The ion probe was tuned to a mass resolving power of 2200, sufficient to separate interferences of ^{18}OH on ^{19}F and $^{16}O_2$ on ^{32}S. No energy filtering was used and the energy slit was kept wide open (±125 eV). A small field aperture was inserted into the secondary ion beam path in order to accept only those ions coming from the central 8 μm of the sputtered crater. This has the effect of filtering out ions from the edge of the crater and the sample surface, resulting in a very low detection limit for H_2O (<30 ppm). Secondary ions (^1H, ^{30}Si, ^{32}S, and ^{35}Cl) were counted by an ETP electron multiplier feeding into an ECL counting system with a deadtime of 13 ns. Secondary ion counts were referenced to counts for ^{30}Si (e.g., $^1H/^{30}Si$, $^{32}S/^{30}Si$). Analytical uncertainty on individual analyses is typically ±10 percent except where low numbers of ions indicate a larger standard deviation. For a detailed discussion of the calibration procedure, the reader is referred to Hauri et al. (2002).

Homogenization of multiphase silicate melt inclusions was performed on a Linkam TS 1500 stage (linked to a TMS 92 programmer) mounted on an Olympus petrographic microscope. All experiments were conducted under flowing nitrogen to minimize oxidation of the sample at high temperature. Samples were heated to 900°C at a rate of 30°C/min; the rate was then decreased to 3°C/min until homogenization at ≈1,210°C. After homogenization, the samples were cooled to 300°C at ≈200°C/min (the fastest cooling rate possible with the stage) to produce a homogeneous glass that could be analyzed by electron microprobe. Sobolev et al. (1990) reported that slow heating rates might affect the compositions of melt inclusions through water loss. However, the good agreement between compositions of glass in heated and quenched inclusions and those of glass in unheated inclusions indicates minor if any changes as a result of heating. It should be noted that

the purpose of the heating experiments was only to produce a homogeneous glass for electron microprobe analysis. Homogenization temperatures are reported simply to indicate the maximum temperature of heating and should not be interpreted as the trapping temperature.

Results

Petrography

All of the samples are vesicular porphyritic andesites. Hand samples range in color from light to dark gray with some alteration evident. Plagioclase, clinopyroxene, and orthopyroxene phenocrysts, and matrix glass are visible in hand samples. In thin section, phenocrysts are euhedral to anhedral and range in size from 0.5 to 3 mm. The order of abundance of phenocrysts is orthopyroxene > plagioclase > clinopyroxene. Minor phases include Ti magnetite and acicular apatite. All phenocrysts appear homogeneous in cross-polarized transmitted light, however, plagioclase phenocrysts exhibit fine-scale chemical zoning when viewed with differential interference contrast microscopy after etching in fluoboric acid (Anderson, 1983). Phenocrysts comprise from 50 to 70 vol percent of most samples. Phenocrysts are surrounded by matrix glass that contains microlites of pyroxene, plagioclase, and Ti magnetite.

Phenocrysts contain both mineral and silicate melt inclusions, with a notable absence of fluid inclusions. Silicate melt inclusions generally range in size from 5 to 50 μm, with the majority ranging between 10 and 25 μm. Shapes of melt inclusions range from spherical to negative crystal shape. The melt inclusions were subdivided into four types based on the phase assemblage observed at room temperature (Fig. 2). Type I inclusions contain only glass; type II inclusions contain glass plus a vapor (shrinkage?) bubble; type III inclusions contain glass plus one or more solids; type IV inclusions contain glass, a vapor bubble, and one or more solids. All four types of inclusions have been observed along growth zones in phenocrysts (Fig. 3A) and as isolated, randomly distributed occurrences throughout crystals. The inclusion assemblages in the 1977, 1988, and 1989 samples appear to be similar, whereas the assemblage in the 1991 sample is noticeably different.In the 1977 to 1989 group of samples, type I all-glass inclusions and type II glass plus vapor inclusions occur in all three phenocryst minerals (plagioclase, orthopyroxene, and clinopyroxene).The type I inclusions are very small (1–5 μm) and abundant in some portions of plagioclase phenocrysts.The vapor bubble in the type II inclusions occupies about 10 vol percent of the inclusions and is very consistent.Type III melt inclusions containing glass and a plagioclase crystal were observed in ortho- and clinopyroxenes in the 1977 to 1989 group of samples, and the glass/crystal ratio was highly variable suggesting that the plagioclase crystals represent trapped solids.The type I inclusions (all glass) are generally smaller than the other inclusions.This suggests that the type I and type II inclusions both trapped the same melt phase, but that a vapor bubble has not nucleated in the smaller type I inclusions, as has been suggested by Roedder (1979).This interpretation is sup-

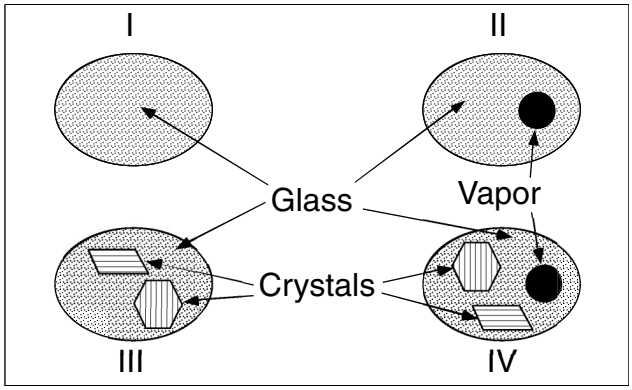

FIG. 2. Schematic representation of the different types of melt inclusions observed in samples from White Island.

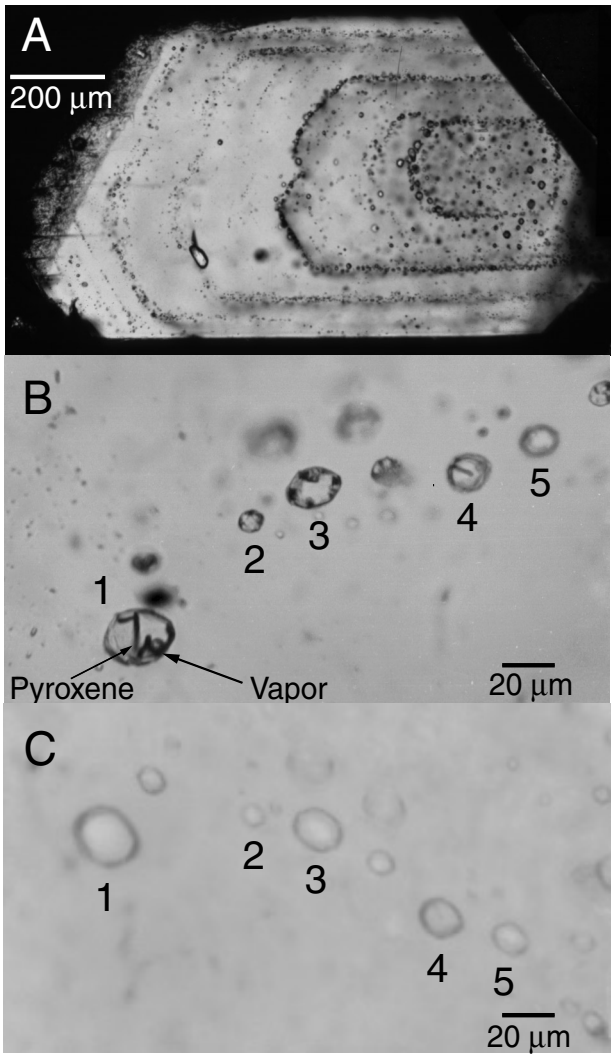

FIG. 3. A. Photomicrograph of orthopyroxene crystal showing several growth surfaces outlined by melt and mineral inclusions. B. Crystallized (type IV) melt inclusions in plagioclase from the 1991 eruption. Each inclusion contains a pyroxene crystal and a vapor bubble. C. Same area shown in (B) after heating the inclusions to homogenization followed by quenching to glass.

ported by compositional data presented below. Wardell et al. (2000) studied melt inclusions in a scoria block erupted in 1989 and reported only types I and II inclusions.

Phenocrysts from the 1991 eruption contain almost exclusively type IV melt inclusions. Among the crystals identified in these inclusions are plagioclase, pyroxene, and Ti magnetite. Unlike the type IV inclusions in the 1977 to 1989 group of samples, the type IV inclusions in the 1991 samples showed uniform phase ratios within a group of presumably contemporaneous inclusions, suggesting that the solids in the 1991 samples are daughter minerals that precipitated from the melt during cooling. This interpretation is supported by the observation that the solids dissolved when the inclusions were heated (Fig. 3B-C). When the homogenized inclusions were quenched and analyzed, their compositions were found to be similar to the all-glass type I inclusions in the 1977 to 1989 samples.

Mineral inclusions are common in phenocrysts from all eruptions. The mineral inclusions are typically larger than melt inclusions, ranging in size from 30 to 150 μm, and in cross section they appear rounded. Inclusions of plagioclase occur in pyroxenes, and both ortho- and clinopyroxene inclusions occur in plagioclase. Silicate melt and mineral inclusions commonly occur within the same phenocryst, as well as in the same growth zone. Petrographically it is difficult to distinguish between mineral inclusions and type I melt inclusions.

Major element chemistry

Pyroxenes: Phenocrysts of orthopyroxene and clinopyroxene plot in the enstatite and augite fields, respectively (Fig. 4A). Analyses from all samples yield a narrow range of compositions: $En_{69–72}$, $Fs_{23–26}$, $Wo_{3–5}$, with Mg# [100Mg/(Mg + Fe_{total})] = 72–76, and $En_{45–46}$, $Fs_{14–16}$, $Wo_{38–40}$, with Mg# = 74–76. Pyroxene inclusions in plagioclase have compositions that are similar to compositions of pyroxene phenocrysts: En72–73, Fs23–24, Wo4, with Mg# = 72–73 and En47–49, Fs13–15, Wo37–39, with Mg# = 76–79 (Fig. 4A). Compositions of pyroxene phenocrysts and mineral inclusions are listed in Table 1.

Plagioclase: Plagioclase phenocrysts range from An_{62} to An_{68} and plot in the labradorite field (Fig. 4B). The compositions of plagioclase inclusions in orthopyroxene (An_{62} to An_{74}) and clinopyroxene (An_{62}–An_{68}) include the range of compositions for plagioclase phenocrysts but extend to higher anorthite contents into the field of bytownite. There is no correlation between the range in An content and the year in which the sample was ejected from the magma chamber.Also, there is no systematic correlation between the An content of plagioclase inclusions and the location of the inclusion within the phenocryst (i.e., there is no systematic zoning in plagioclase composition from cores to rims of phenocrysts). Compositions of plagioclase phenocrysts and mineral inclusions are listed in Table 2.

Melt inclusions: Composition ranges and averages, and CIPW norms of melt inclusions hosted in all three phenocryst minerals (plagioclase, orthopyroxene, and clinopyroxene) are listed by eruption year in Table 3 and by host phase in Table 4. Compositions of melt inclusions trapped in samples from the 1977, 1986, 1988, and 1989 eruptions (77/89) are similar and independent of host phase (Fig. 5) or year in which they were erupted (Fig. 6). No correlation was found between the location of the inclusion in the host mineral and the composition of the melt (Fig. 7). Glass in unhomogenized multiphase melt inclusions from 1991 has a composition that differs from compositions and CIPW norms of glass in samples from the other 4 yr. However, compositions of homogenized melt inclusions in clinopyroxene from 1991 are similar to the 77/89 compositions with the exception of the alkalis, which are lower in the 1991 sample (Table 3). Analytical totals for the glasses range from 93 to 99 percent, which is interpreted to indicate the presence of unanalyzed volatiles in the melts and/or loss of sodium during the analysis (Morgan and London, 1996).

Matrix glass: Matrix glass has a composition similar to that of glass in melt inclusions from the 77/89 samples (Figs. 5–6) and similar to glass in homogenized 1991 melt inclusions. Microlites in matrix glass have compositions that are similar to compositions of phenocrysts in the same samples (Fig. 4).

Copper and zinc abundances in melt inclusions

Two melt inclusions in pyroxene, three melt inclusions in plagioclase, and matrix glass from the sample erupted in 1977 were analyzed for copper (Rapien, 1998). The three inclusions in plagioclase were also analyzed for zinc.

Copper concentrations determined for the two inclusions in orthopyroxene are 245 ± 35 ppm (n = 21 spots) and 160 ± 30 ppm (n = 5 spots). The copper concentration of the melt inclusion in plagioclase analyzed by electron microprobe ranged from 104 to 386 ppm (n = 11 spots), and the concentration of zinc in this same inclusion was 150 ppm. Two inclusions in plagioclase analyzed by synchrotron XRF contained 644 ± 30 and 731 ± 35 ppm copper, and 96 ± 5 and 98 ± 5 ppm zinc, respectively. While the copper and zinc concentrations show some variability between inclusions, the concentrations of both of these metals are clearly elevated in the melt inclusions relative to the host phase concentrations, as evidenced by the electron microprobe traverse shown in Figure 8. Copper in matrix glass was generally lower than that in melt inclusions, with a range of 170 to 220 ppm and an average of 188 ppm (n = 5). Cole et al. (2000) report whole-rock copper values at White Island ranging from 33 to 93 ppm (n = 12), with an average of 64 ppm. For comparison, the average copper concentration in andesites is reported to be 60 ppm, with a range from 10 to 150 ppm (Gill, 1981).

Trace elements

Melt inclusions and matrix glass from the 1988 and 1989 samples were analyzed for trace elements (Table 5). The melt inclusions were hosted by orthopyroxene, clinopyrox-

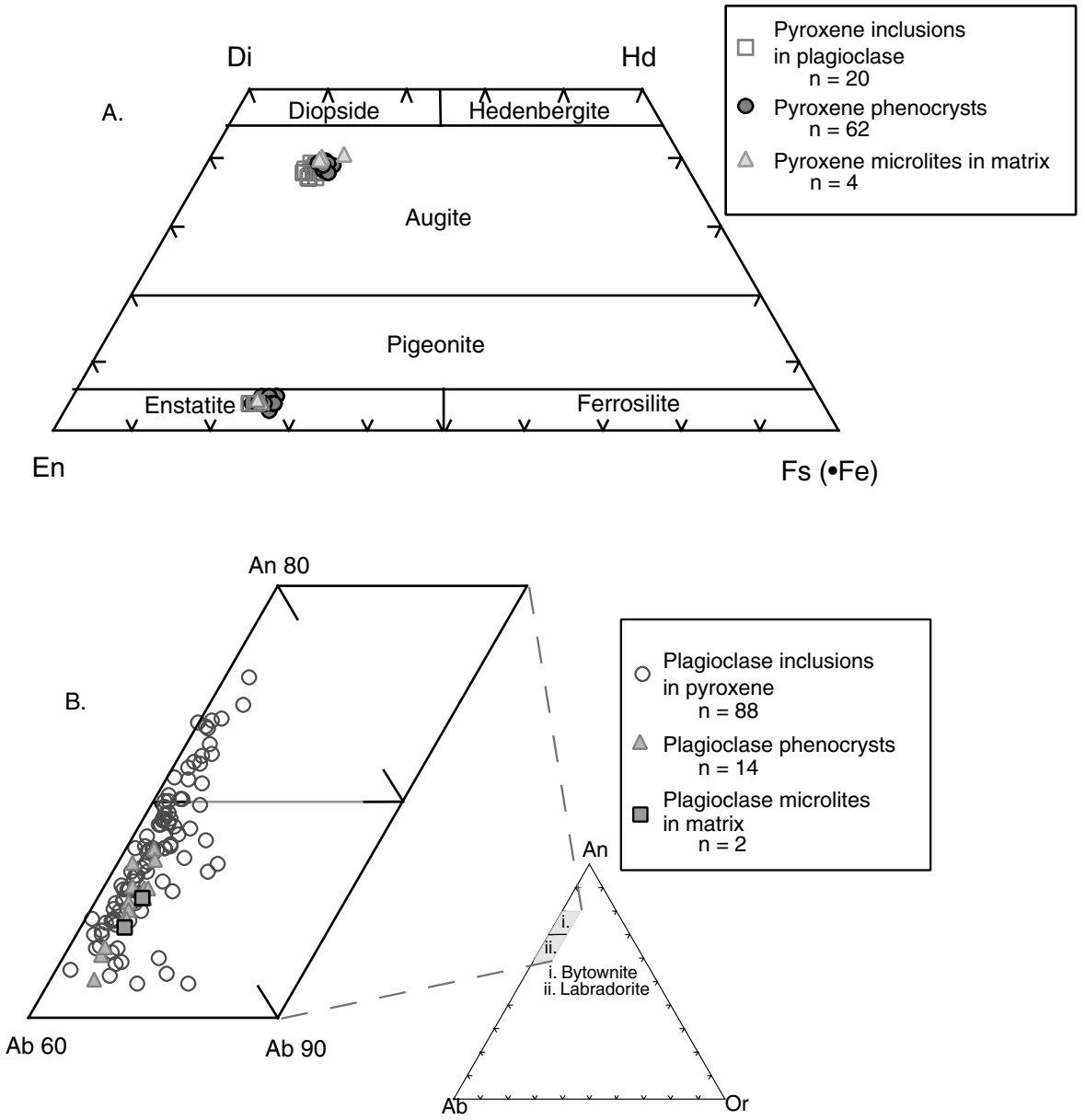

FIG. 4. Compositions of phenocrysts, mineral inclusions, and matrix glass microlites for pyroxene (A) and plagioclase (B) determined by electron microprobe. Pyroxene nomenclature after Morimoto (1988).

ene, and plagioclase. Trace element concentrations for the inclusions show no significant variation as a function of host phase (Table 5). Trace element concentrations of matrix glass are similar to melt inclusion glass, except that matrix glass lacks a positive Eu anomaly (Fig. 9). While the europium content of igneous rocks is usually interpreted in terms of fractionation between melt and plagioclase, at White Island Eu chemistry may also be affected by melt-volatile partitioning. Flynn and Burnham (1978) showed that although the trivalent rare earth elements are all partitioned into the melt phase relative to the coexisting aqueous chloride fluid, Eu shows much weaker fractionation than the other rare earths.More recently, Reed et al. (2000) showed that while the partition coefficient for all REE increases with increasing salinity at 800°C and 2,000 bars, partitioning of Eu relative to the other REE decreases with increasing salinity. Thus, separation of a low-salinity magmatic aqueous fluid during degassing at White Island could have produced matrix glass that was depleted in Eu relative to the other REE.

Volatiles

Volatile-component concentrations were determined in the same melt inclusions and matrix glass that were ana-

TABLE 1. Electron Microprobe Analyses (wt %) of Pyroxene Phenocrysts and Mineral Inclusions (numbers in italics represent the range for all *n* analyses)

	Clinopyroxene phenocryst *n* = 22	Clinopyroxene inclusions in plagioclase *n* = 15	Orthopyroxene phenocryst *n* = 40	Orthopyroxene inclusions in plagioclase *n* = 5
SiO_2	52.71 *50.93–54.87*	52.15 *50.97–53.26*	53.81 *51.73–55.72*	51.66 *48.75–54.2*
TiO_2	0.49 *0.39–0.63*	0.44 *0.30–0.60*	0.23[1] *0.09–0.34*	0.28 *0.20–0.30*
Al_2O_3	1.85 *1.58–2.08*	1.93 *1.79–2.00*	1.14 *0.82–1.52*	1.13 *1.07–1.24*
MgO	16.15 *15.53–16.60*	17.19 *16.51–17.80*	26.13 *25.3–27.14*	26.74 *25.86–27.77*
CaO	18.94 *18.25–19.72*	18.98 *18.16–19.44*	2.10 *1.7–2.6*	2.02 *1.86–2.14*
MnO	0.37 *0.27–0.46*	na	0.41 *0.17–0.67*	Na
FeO	9.72 *9.08–10.35*	8.78 *8.07–9.63*	16.44 *15.11–18.38*	15.12 *14.90–15.35*
Na_2O	0.22 *0.14– 0.33*	0.27 *0.16–0.35*	0.04 *Bd–0.11*	0.06 *0.10–0.07*
K_2O	bd	0.04 *bd–0.09*	Bd	0.04 *bd– 0.06*
F	0.14 *bd–0.34*	na	0.10[1] *bd–0.32*	Na
Cl	bd	na	Bd	Na
Total	100.62 *97.46–103.25*	99.78 *97.58–100.71*	100.42 *97.46–103.25*	97.05 *93.52–100.68*

Notes: bd = below detection limits, na = not analyzed for those samples
[1] Number analyzed is less for this value

TABLE 2. Electron Microprobe Analyses (wt %) of Plagioclase Phenocrysts and Mineral Inclusions (numbers in italics represent the range for all *n* analyses)

	Plagioclase phenocryst *n* = 14	Plagioclase inclusions in clinopyroxene *n* = 14	Plagioclase inclusions in orthopyroxene *n* = 74
SiO_2	51.65 *48.53–53.14*	51.85 *49.72–55.19*	51.41 *48.67–55.96*
TiO_2	0.05 *bd–0.10*	0.09 *0.04–0.26*	0.11[1] *bd–0.37*
Al_2O_3	29.09 *28.75–29.50*	28.92 *24.34–31.58*	29.10 *24.99–31.11*
MgO	0.16 *0.10–0.23*	0.65 *0.16–3.08*	0.36 *0.08–1.90*
CaO	13.35 *12.68–14.15*	13.86 *12.31–15.32*	13.41 *10.97–14.81*
MnO	0.06[1] *bd–0.13*	0.09 *bd–0.15*	0.10 *bd–0.36*
FeO	0.71 *0.59–0.89*	1.36 *0.81–2.79*	1.58 *0.86–3.08*
Na_2O	3.76 *3.54–4.13*	3.34 *2.61–3.74*	3.48 *2.75–4.44*
K_2O	0.25 *0.11–0.33*	0.26 *0.15–0.61*	0.24[1] *0.05–0.85*
F	0.141 *bd–0.46*	0.03 *bd–0.14*	0.13[1] *bd–0.30*
Cl	bd	bd	Bd
Total	99.19 *95.83–100.81*	100.44 *98.15–101.82*	99.71 *96.79–101.98*

Notes: bd = below detection limits, na = not analyzed for those samples
[1] Number analyzed is less for this value

lyzed for trace elements. Calculated volatile concentrations are listed in Table 6, along with the equations used to obtain those values. Algorithms used to reduce the ion probe data are those that were appropriate for the instrument at the Department of Terrestrial Magnetism at the time the analyses were conducted (Erik Hauri, pers. commun., 1999; see also Hauri et al., 2002).

Water contents (Fig. 10) are consistently higher in the melt inclusions (0.27–0.89 wt %), compared to the matrix glass (0.07–0.20 wt %), suggesting that the matrix glass lost water during eruption, as might be expected. Similar results were reported by Wardell et al. (2000; Fig. 10).

The Cl content of matrix glass is highly variable, with some values higher and some lower than melt inclusion concentrations. Similar results were reported by Wardell et al. (2000). Matrix glass generally has a lower S concentration (0.3–58 ppm) compared to melt inclusions (31–88 ppm), suggesting near-surface loss of sulfur from the melt (matrix glass) during eruption. Melt inclusion and matrix glass sulfur concentrations lie at the low end of the range of sulfur values reported for blocks and bombs erupted at White Island in 1977—these were generated from degassed magma and contain between 30 and 250 ppm S (as reported in Houghton and Nairn, 1989b).

Discussion

Although the year in which each sample was erupted from the magma chamber is known, it is not possible to determine when the individual phenocrysts in the ejecta formed, or when the mineral and melt inclusions were trapped in individual phenocrysts. Each phenocryst and its melt and mineral inclusions is therefore considered to represent a random sampling of the phases that were present in the magma chamber at some unknown location and time in the past. Petrographic and electron microprobe data indicate that plagioclase, orthopyroxene, and clinopyroxene were the only major phases crystallizing during the unknown magma residence time represented by the ejecta. Each of the three phenocrysts occurs as mineral inclusions in at least one other type of phenocryst, and the mineral inclusions have compositions that are similar to the compositions of phenocrysts of that mineral in the same sample. The compositions of plagioclase, orthopyroxene, and clinopyroxene are independent of their mode of occurrence. That is, phenocrysts of a given phase have the same composition as solid inclusions of that same phase. This is interpreted to indicate that all three phenocryst minerals were in equilibrium and precipitating from the melt at the

TABLE 3. Major Element Compositions (wt %) of Melt Inclusions Determined by Electron Microprobe (numbers in italics represent the range for all *n* analyses; CIPW norms were calculated for the averages given in the table)

	1977 average *n* = 14	1986 average *n* = 16	1988 average *n* = 25	1989 average *n* = 20	1991 average unhomogenized *n* = 19	1991 average homogenized *n* = 9
SiO_2	64.25 *61.07 -66.12*	63.75 *62.87–64.59*	63.88 *59.99–65.87*	64.23 *61.28–67.25*	68.28 *63.24–71.39*	64.88 *63.11–66.54*
TiO_2	1.18 *0.68–1.6*	1.08 *0.95–1.20*	0.96 *0.70–1.30*	1.08[1] *0.90–1.40*	1.00 *0.65–1.49*	1.33 *1.04–1.50*
Al_2O_3	12.68 *11.3–13.80*	13.81 *13.36–14.27*	14.39 *13.35–15.83*	13.67 *13.17–14.58*	14.68 *12.57–16.2*	13.41 *12.48–14.94*
MgO	1.93 *0.98–2.43*	2.16 *1.96–2.31*	2.07 *1.43–2.63*	1.96 *0.81–2.56*	0.9 *0.14–4.06*	1.81 *1.62–2.01*
CaO	4.70 *4.08–5.60*	5.14 *4.55–5.55*	5.13 *4.43–5.97*	4.85 *3.73–6.15*	3.05 *2.1–4.55*	5.44 *5.06–5.89*
MnO	0.15 *0.05–0.29*	0.09 *0.02 -0.21*	0.17 *0.12–0.26*	0.14[1] *0.12–0.30*	0.07 *bd–0.17*	0.20 *0.09–0.28*
FeO	7.05 *6.27–7.84*	6.19 *5.45 -6.88*	6.42 *5.22–7.94*	6.31 *5.25–7.68*	2.15 *1.29–3.79*	8.08 *7.35–8.53*
Na_2O	2.45 *1.75–3.13*	2.87 *2.50–3.08*	2.60 *1.79–3.18*	2.24 *1.54–2.99*	2.06 *1.24–3.27*	0.87 *0.54–1.24*
K_2O	2.87 *2.54–3.11*	2.49 *2.30–2.68*	2.66 *1.86–3.24*	2.58 *1.74–2.84*	2.77 *1.91–3.53*	1.71 *1.50–1.97*
F	0.07 *bd–0.20*	0.13 *bd–0.30*	0.05 *bd–0.17*	na	0.11 *bd–0.29*	0.04 *Bd–0.17*
Cl	0.14 *0.14–0.08*	0.12 *0.09–0.18*	0.13 *0.09–0.17*	na	0.27 *0.10–0.82*	0.14 *0.11–0.18*
Total	97.45 *97.45–99.11*	97.83 *96.72–98.59*	98.46 *94.62–99.95*	96.72 *93.41–99.01*	95.34 *91.94–97.78*	97.90 *94.60–99.47*
Q	27.49	24.96	25.31	28.84	40.05	38.70
C	0.00	0.00	0.00	0.00	3.87	0.92
Or	16.94	14.70	15.70	15.23	16.35	10.09
Ab	19.68	23.38	21.02	17.91	15.42	6.32
An	15.65	17.89	20.22	20.14	13.11	25.64
Di	4.99	4.46	3.13	1.64	0.00	0.00
Hy	4.75	5.16	5.90	6.03	2.23	6.99
Il	2.24	2.05	1.83	2.05	1.90	2.53
Mt	4.60	4.05	4.19	4.12	1.09	5.28
Hm	0.00	0.00	0.00	0.00	0.22	0.00
Ap	0.44	0.44	0.44	0.44	0.44	0.44
Hl	0.23	0.2	0.21	0.23	0.44	0.23
Fl	0.10	0.18	0.07	0.14	0.15	0.06

Notes: bd = below detection limits, na = not analyzed for those samples
[1] Number analyzed is less for this value

same time. Moreover, since the phenocrysts and their mineral and melt inclusions presumably represent trapping over some unknown but extended period of time and location within the magma chamber, the data suggest that the magma chamber was relatively well mixed and that crystallization did not significantly change the composition of the melt during the time period sampled by the melt inclusions.

The relative chronology of trapping of melt or mineral inclusions within a crystal can be estimated based on position within the crystal, with melt inclusions toward the core presumably trapped earlier than those found near the edge. This interpretation obviously only applies to primary inclusions trapped during growth of the crystal and does not apply to secondary inclusions in the crystals. However, no significant change in melt chemistry as a function of position within the crystal was observed for primary inclusions along growth zones. Plagioclase inclusions, which have variable chemistry (Fig. 4B), show no systematic

TABLE 4. Major Element Compositions (wt %) of Melt Inclusions Grouped by Phenocryst Host (numbers in italics represent the range for all *n* analyses; CIPW norms were calculated for the averages given in the table)

	Melt inclusions in clinopyroxene *n* = 22	Melt inclusions in orthopyroxene *n* = 17	Melt inclusions in plagioclase *n* = 33
SiO_2	63.44 *59.99–65.44*	64.34 *61.97–65.87*	64.19 *31.07–67.25*
TiO2	1.02 *0.70–1.30*	0.96 *0.68–1.14*	1.13 *0.90–1.60*
Al2O3	14.05 *13.35–15.83*	14.03 *13.22–15.21*	13.31 *11.30–14.27*
MgO	2.12 *1.75–2.63*	1.65 *0.81–2.36*	2.16 *1.30–2.56*
CaO	5.20 *4.43–5.97*	5.29 *4.53–6.15*	4.65 *3.73–5.42*
MnO	0.14 *0.002–0.23*	0.17[1] *bd–0.30*	0.11[1] *0.05–0.19*
FeO	6.44 *5.22–7.94*	6.79 *5.74–7.68*	6.32 *5.25–7.84*
Na2O	2.75 *1.79–3.09*	2.51 *1.75–3.18*	2.42 *1.54–2.42*
K_2O	2.57 *1.86–3.24*	2.60 *1.74–2.84*	2.70 *2.37–3.11*
F	0.07 *bd–0.30*	0.07[1] *bd–0.20*	0.10[1] *bd–0.30*
Cl	0.12 *0.09–0.16*	0.13[1] *0.08–0.18*	0.13[1] *0.09–0.22*
Total	97.93 *94.62–99.34*	98.53 *95.87–99.95*	97.08 *93.41–99.11*
Q	24.54	27.00	27.68
Or	15.17	15.35	15.94
Ab	22.37	20.26	19.50
An	18.84	19.82	17.96
Di	4.40	3.96	2.63
Hy	5.36	4.67	6.01
Il	1.94	1.83	2.15
Mt	4.21	4.44	4.12
Ap	0.44	0.44	0.44
Hl	0.20	0.21	0.21
Fl	0.10	0.10	0.14

Notes: bd = below detection limits, na = not analyzed for those samples
[1] Number analyzed is less for this value

change in composition from cores to rims of phenocrysts. The range in An content of plagioclase inclusions is about as large within a single domain (i.e., core, middle, rim) of a single crystal as it is within the entire crystal, and the range within a single crystal is about the same as the complete range observed in all the crystals. The fact that the composition of plagioclase inclusions varies from An_{62} to An_{74}, and that the compositions of plagioclase phenocrysts show the same range, and that the range in plagioclase composition appears to be independent of scale (i.e., individual growth zone, individual crystal, individual sample, all samples) suggests that the plagioclase phenocrysts and inclusions were trapped within a convecting, relatively homogeneous magma chamber. Such a scenario is consistent with that proposed by Shinohara and Hedenquist (1997) for crystallization of shallow magma chambers associated with porphyry copper deposits.

As noted above, melt inclusions in the 1991 sample differ petrographically from inclusions in the earlier eruption samples. Specifically, the 1991 inclusions contain daughter minerals, whereas daughter minerals were absent from inclusions from all other eruptions. Several possible explanations exist for the observed difference between the 1991 sample and those from the earlier eruptions. It is well known that the phase assemblage in a melt inclusion is a function of both the inclusion size and the cooling rate (Roedder, 1979; Lowenstern, 1995). For a given composition and cooling rate, larger inclusions are more likely to nucleate a vapor bubble and/or daughter minerals during cooling, whereas smaller inclusions often fail to nucleate any phases and remain as one-phase glass inclusions at room temperature. However, size is unlikely to be the cause of the observed difference between the 1991 sample and earlier samples because melt inclusions in the 1991 sample are not noticeably larger than inclusions in other samples. For a given composition and inclusion size, slower cooling is more likely to cause vapor bubbles and/or daughter minerals to nucleate. Although we cannot test this hypothesis, it is possible that the 1991 samples experienced a different P-T history than the other samples. Possible scenarios that could result in a different P-T history might be a longer residence time in the magma following entrapment, and/or a slower cooling history after entrapment (either in the magma chamber or after eruption to the surface), and/or eruption from a different location within the magma chamber (i.e., from the core or the periphery of the chamber). An alternative explanation for the presence of daughter minerals in the 1991 samples, and their absence from the other samples, is that the 1991 samples trapped a melt of different composition. However, the composition of homogenized melt inclusions from the 1991 samples is similar to that of glass in the 1977 to 1989 group of samples, indicating that both types of inclusions trapped the same melt.

White Island has been characterized as a quiescently erupting volcano in which there have been repeated discharges of ash and vapor over an extended period of time. Hedenquist (1995) reports that the flux of magmatic volatiles from explosively and quiescently erupting arc volcanoes is about the same when integrated over a period of 100 yr (although the 100-yr total amount of volatiles from explosive volcanoes may be discharged over a period of a few months to a few years, whereas the discharge from quiescent volcanoes is relatively continuous over the 100-yr period). In contrast to the flux of volatiles, the flux of metals from quiescent volcanoes is smaller compared to explosive volcanoes. Hedenquist (1995; see also Giggenbach, 1987) relates these differences to aqueous phase immiscibility in the deeper portions of quiescent systems. In this model, most of the metal is partitioned into the high-salin-

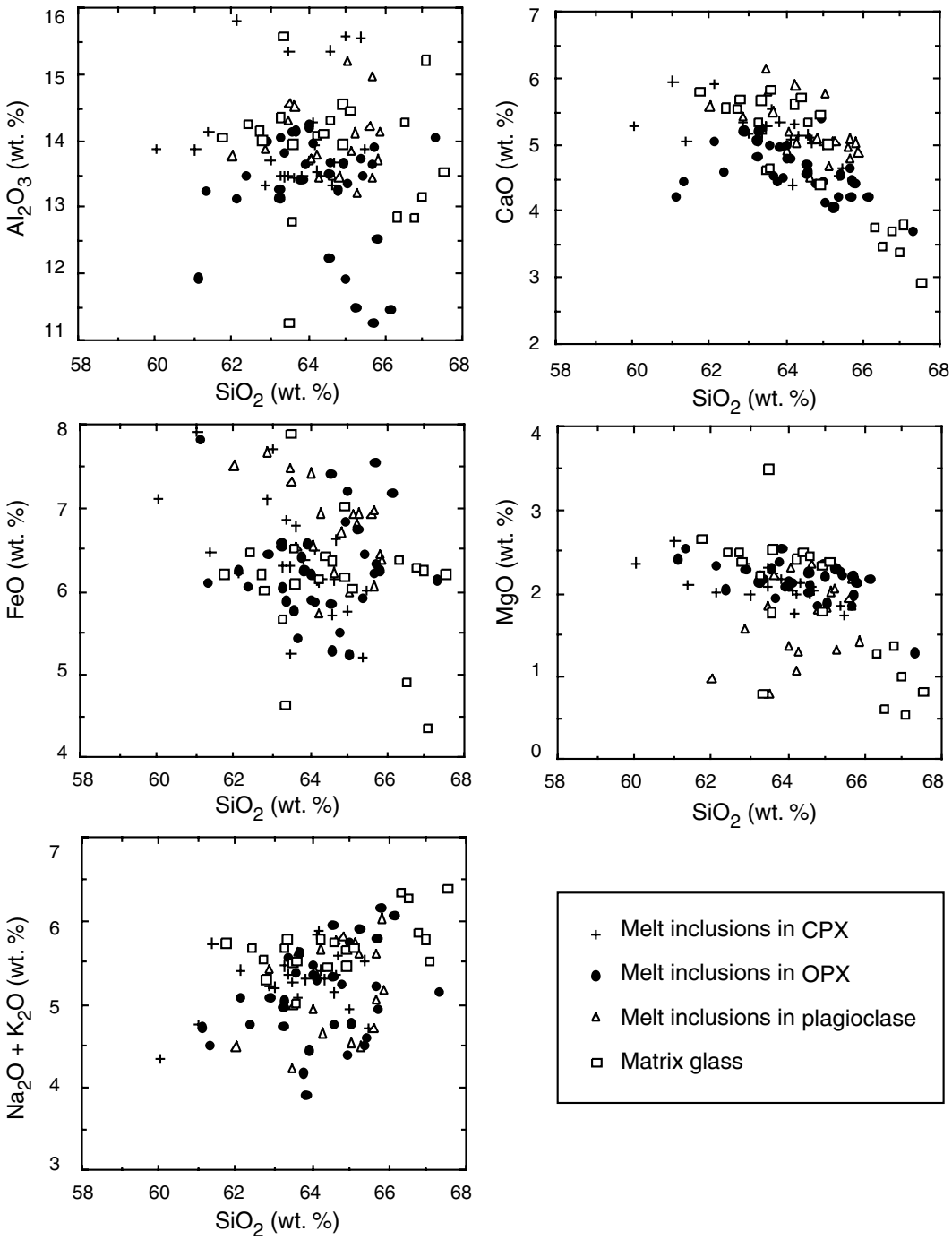

FIG. 5. Harker variation diagrams for melt inclusions grouped according to host phase. Also shown are data for matrix glass.

ity liquid, resulting in a relatively metal-poor vapor that escapes through the top of the volcano (Bodnar, 1982; Beane and Bodnar, 1995). The metal-rich liquid remains in the deeper portions of the system to form porphyry copper-type mineralization. Assuming the current rate of copper discharge from White Island is typical of the discharge rate over the 10,000-yr life of the volcano, approximately 1 Mt Cu would have been discharged into the atmosphere (Hedenquist et al., 1993; Hedenquist, 1995). While this appears to be a large amount of Cu, considering that the total tonnage in economic porphyry copper deposits ranges from <100,000 t to >45 Mt (Clark, 1993), this amount only represents loss of about 330 ppm of Cu from a 1 km^3 magma chamber in 10,000 yr or only 33 ppm loss from a 10 km^3 magma chamber. The relatively low Cu content of volcanic gases at White Island is consistent with ana-

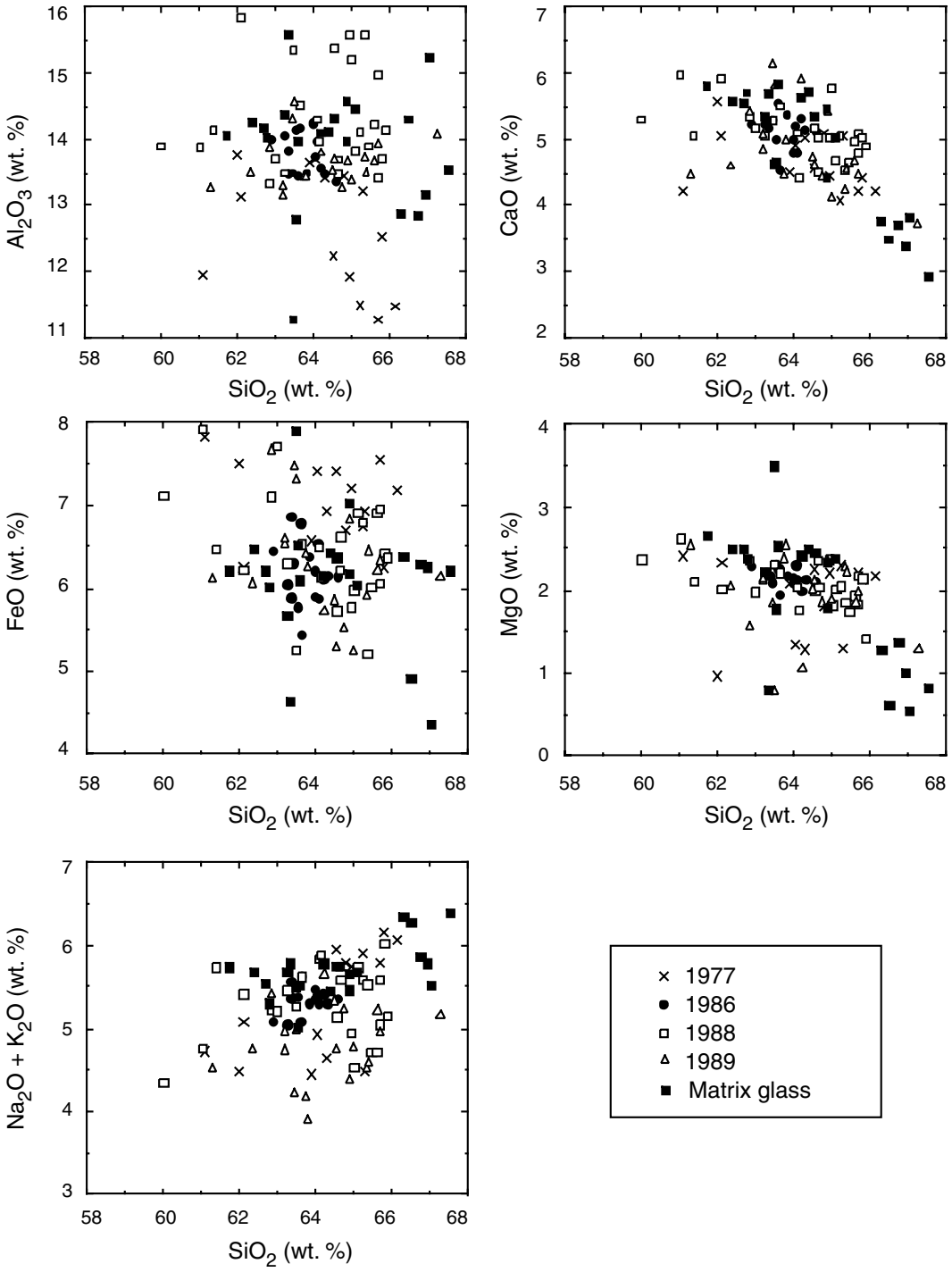

FIG. 6. Harker variation diagrams for melt inclusions grouped according to year of eruption. Also shown are data for matrix glass.

lytical results from melt inclusions reported here. At any P-T condition reasonable for the White Island magma chamber, chlorine (and chloride-complexed metals) will be partitioned into the magmatic volatile phase relative to the melt (Kilinc and Burnham, 1972; Candela, 1989; Cline and Bodnar, 1991; Shinohara, 1994). Yet, the Cl/H_2O ratio ($\approx$0.016) of the vapor discharging from White Island is about an order of magnitude lower than the Cl/H_2O ratio of the melt inclusions ($\approx$0.15).This suggests that magmatic aqueous phase immiscibility is occurring at depth, and that most of the metal that is being discharged from the magma remains in the deeper parts of the system (cf. Bodnar, 1982;

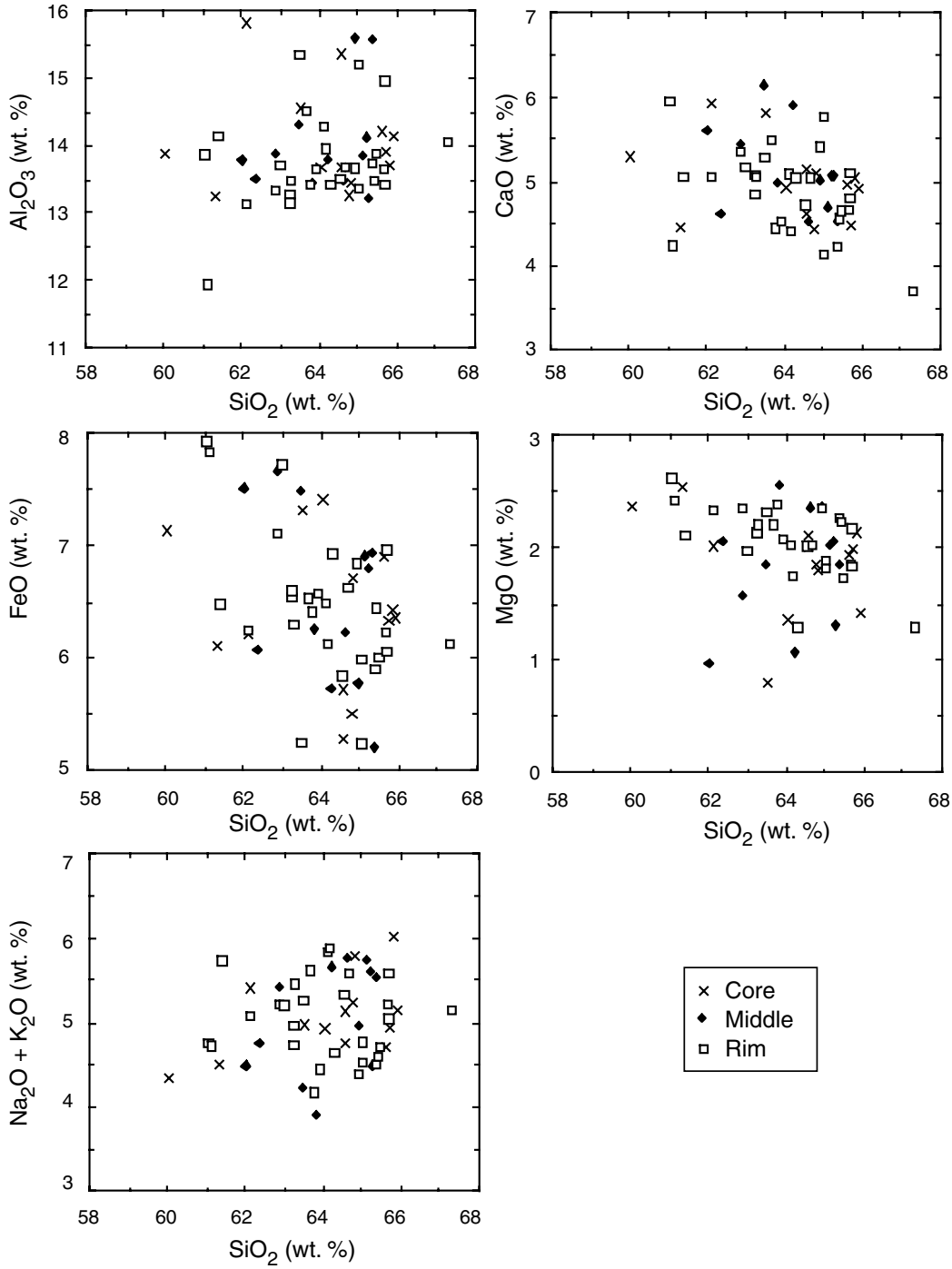

FIG. 7. Harker variation diagrams for melt inclusions grouped according to location within host phenocryst.

Giggenbach, 1987), where it is available to produce porphyry copper-type mineralization.

Is there a porphyry copper deposit in White Island's future?

The generally accepted model for the formation of porphyry copper deposits involves the emplacement and crystallization of a hydrous silicic magma at shallow levels in the earth's crust (Burnham, 1979, 1997). During crystallization, the water concentration of the melt increases, eventually reaching saturation and resulting in exsolution of a magmatic aqueous phase.Chlorine, copper, and other metals are partitioned into the magmatic aqueous phase (Burnham, 1979; Candela, 1989; Bodnar, 1995) and metals are later deposited in veins as the magmatic fluids cool and/or

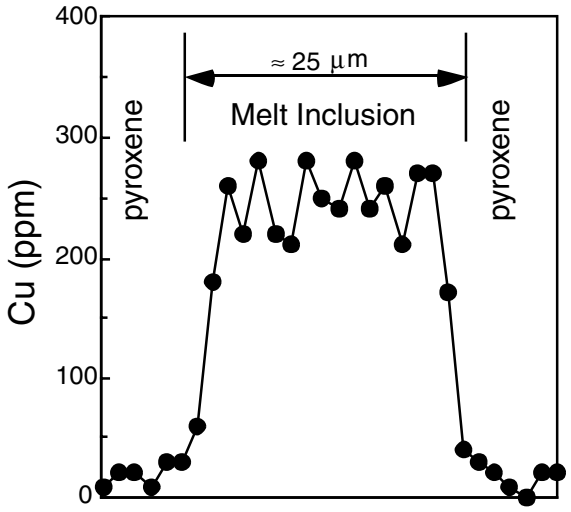

FIG. 8. Electron microprobe traverse for copper across melt inclusion in pyroxene.

TABLE 5. Trace Element Concentrations (parts per million) of Melt Inclusions and Matrix Glass Determined by Ion Microprobe

	Melt inclusion in orthopyroxene $n = 2$	Melt inclusion in clinopyroxene $n = 1$	Melt inclusion in plagioclase $n = 1$	Matrix glass $N = 5$
Ba	808	734	594	750
Rb	58	56	29	47
Nb	7	6	5	6
La	14	14	12	14
Ce	30	31	25	30
Sr	135	115	172	144
Be	1	2	2	1
Nd	15	16	13	14
Hf	6	6	3	6
Zr	177	155	142	178
Sm	3	5	6	4
Eu	3	5	2	1
Gd	4	5	3	3
Ti	5,377	4,825	4,463	5,121
Dy	4	8	5	5
Er	2	2	3	3
Y	21	28	22	22
Yb	18	4	5	3
Li	17	17	15	16
Sc	30	33	17	15
Cr	85	292	25	33

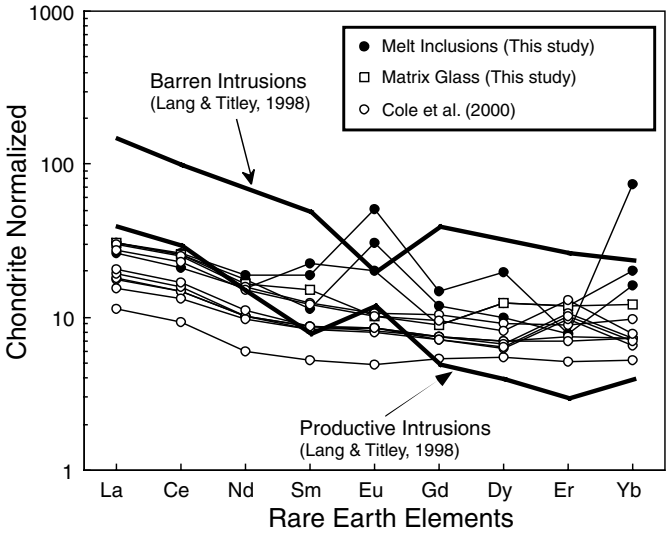

FIG. 9. Chondrite-normalized rare earth element (REE) concentrations in melt inclusions and matrix glass from this study. Also shown are whole-rock data for White Island from Cole et at. (2000) and the REE patterns characteristic of barren and productive porphyry copper intrusions from Lang and Titley (1998). Chondritic values are from Anders and Grevasse (1989).

mix with lower salinity hydrothermal fluids (Beane and Bodnar, 1995). As a result of numerous theoretical, experimental, and field studies of the porphyry copper environment, we now have a fairly detailed understanding of the physical and chemical features that are associated with the formation of economic porphyry copper mineralization (Candela, 1989; Cline and Bodnar, 1991; Lang and Titley, 1998).

Although there appear to be genetic links between shallow high-sulfidation Cu-Au deposits and deeper porphyry-style mineralization at places such as Red Mountain, Arizona (Bodnar and Beane, 1980), and Far Southeast-Lapanto in the Philippines (Hedenquist et al., 1998), the timing of formation of these two types of mineralization is not clear. While Hedenquist et al. (1998, p. 384) report that "K-silicate alteration at depth and quartz-alunite alteration of the epithermal deposit formed contemporaneously at ~1.4 Ma" in the Far Southeast-Lapanto system, the total uncertainty in the age dates (±80 ka) is 16 times greater than the entire history (~10 ka) of the active White Island system and might not be able to discriminate between two events separated in time by only a few kiloannums. Thus, although it has been suggested that high-sulfidation Cu-Au mineralization is presently forming in the shallow subsurface at White Island (Giggenbach, 1987; Hedenquist et al., 1993), it is unclear whether the deeper levels of the White Island system have reached the productive stages of porphyry copper formation. White Island has been an active magmatic-hydrothermal system for about 10,000 yr (Giggenbach and Glasby, 1977), and the magma beneath White Island is probably still dominantly molten (Houghton and Nairn, 1989b). Numerous field studies, as well as fluid inclusion and stable isotope studies of porphyry copper deposits, indicate that the main stage of copper mineralization occurs relatively late in the magmatic history after most of the melt has crystallized.Numerical models by Norton (1982) suggest that for a single emplacement of melt, it takes about 20,000 to 30,000 yr for an approximately 13-km^3 pluton to cool below its solidus. Thus, the deeper White Island magmatic-hydrothermal system may not yet have evolved to the porphyry copper formation stage.

If porphyry copper mineralization is not currently forming at depth at White Island, what is the likelihood that such mineralization will develop in the future? If we assume

TABLE 6. Volatile Concentrations of Melt Inclusions and Matrix Glass Determined by Ion Microprobe

$\left[\frac{^{n}x^{-}}{^{30}Si^{-}}\right]$	MI in 1988 CPX	MI in 1988 CPX	MI in 1988 OPX	MI in 1988 OPX	MI in 1989 Plag	1988 Matrix	1988 Matrix	1989 Matrix	1989 Matrix	1989 Matrix
Cl	0.59	0.48	1.03	1.04	0.75	1.02	1×10^{-3}	1×10^{-3}	0.91	0.80
S	0.08	0.09	0.07	0.14	0.05	0.09	4×10^{-4}	5×10^{-4}	0.02	0.02
H	0.45	0.44	1.04	0.57	0.32	0.18	0.01	5×10^{-3}	0.21	0.14
Wt percent	MI in 1988 CPX	MI in 1988 CPX	MI in 1988 OPX	MI in 1988 OPX	MI in 1989 Plag	1988 Matrix	1988 Matrix	1989 Matrix	1989 Matrix	1989 Matrix
Cl	0.06	0.05	0.10	0.10	0.07	0.09	0.08	0.10	1×10^{-4}	9×10^{-5}
S	0.01	0.01	0.01	0.01	4×10^{-3}	1×10^{-3}	1×10^{-3}	0.01	3×10^{-5}	4×10^{-5}
H_2O	0.42	0.36	0.89	0.46	0.27	0.20	0.15	0.18	0.07	0.07

$$\text{Cl(ppm)} = 736\left[\frac{^{35}Cl^{-}}{^{30}Si^{-}}\right]_N \qquad \text{S(ppm)} = 630\left[\frac{^{32}S^{-}}{^{30}Si^{-}}\right]_N$$

$$\text{Silicic glass } H_2O \text{ (wt\%)} = 0.103 + 0.332\left[\frac{^{1}H^{-}}{^{30}Si^{-}}\right]_N + 0.0544\left[\frac{^{1}H^{-}}{^{30}Si^{-}}\right]_N^2$$

$$\text{Mafic glass } H_2O \text{ (wt\%)} = 0.039 + 0.55667\left[\frac{^{1}H^{-}}{^{30}Si^{-}}\right]_N + 0.17787\left[\frac{^{1}H^{-}}{^{30}Si^{-}}\right]_N^2$$

$$\text{Where}\left[\frac{x}{^{30}Si^{-}}\right]_N = \left[\frac{x}{^{30}Si^{-}}\right] \times \frac{\text{Si value in sample}}{50 \text{ (Si value for mafic magma)}}$$

Abbreviations: CPX = clinopyroxene, MI = melt inclusions, OPX = orthopyroxene, Plag = plagioclase

Notes: Values in the upper portion of the table are uncorrected ion ratio output from the ion probe; values in the lower portion of the table are compositions (wt %) calculated using the equations listed below; reported water value is interpolated between the calculated mafic and silicic values based on silica content; the analytical procedure is described by Hauri et al. (2002)

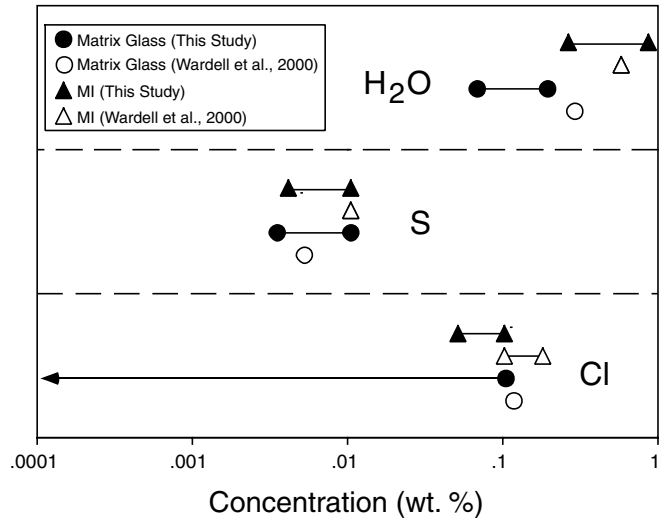

FIG. 10. Volatile (H_2O, S, Cl) component concentrations in melt inclusions and matrix glass from this study. Also shown are data for melt inclusions and matrix glass from Wardell et al. (2000).

that the melt found in melt inclusions in this study is the same melt that will continue to evolve and eventually crystallize to form an intrusive body at depth beneath White Island, we can compare the chemical characteristics of the melt inclusions to observations from known porphyry copper deposits, as well as with similar but barren or subeconomic intrusive rocks. Certainly the copper concentration of the melt is sufficiently high to generate ore-forming fluids. Burnham (1997) has calculated that 32 percent partial melting of a normal tholeiite containing 75 ppm copper will produce a melt with about 230 ppm copper, similar to the values of several hundred ppm in melt inclusions from White Island and considerably higher than the 50 ppm required to form economic concentrations of copper in various models for porphyry copper formation (Candela, 1989; Cline and Bodnar, 1991). Moreover, simple melt-aqueous fluid partition calculations (Bodnar, 1982; Candela and Piccoli, 1995; Burnham, 1997), experimental studies (Williams et al., 1995), and analyses of fluid inclusions from ore deposits (Heinrich et al., 1992, 1999; Audétat et al, 2000) show that copper concentrations in magmatic fluids exsolved from such melts can have copper concentrations of thousands of ppm (summarized in Bodnar, 1999).

Feiss (1978) and Mason and Feiss (1979) measured the $Al_2O_3/(Na_2O + K_2O + CaO)$ ratios of rocks from a number of productive and barren intrusions, including many from the southwest Pacific region. They found that intrusive rocks associated with productive porphyry systems are peraluminous and have higher ratios than those associated with barren systems. More specifically, most mineralized systems have ratios above about 1.3, whereas ratios lower than this are characteristic of barren systems. Using the average concentrations of Al_2O_3, Na_2O, K_2O, and CaO listed in Table 3, all of the melt inclusions from White Island have

$Al_2O_3/(Na_2O + K_2O + CaO)$ ratios ≥1.3, and the glass in the unhomogenized melt inclusions from 1991 has a value of 1.9. If we consider this glass composition to represent the melt composition in the future magma chamber after further crystallization, the $Al_2O_3/(Na_2O + K_2O + CaO)$ ratio of the magma beneath White Island is characteristic of rocks associated with economic porphyry copper mineralization elsewhere. Similarly, Urabe (1985) has shown that partitioning of metals into the magmatic aqueous phase is higher for aluminous (corundum normative) melts than for alkaline melts, and the residual melt (glass) in the 1991 samples contains 3.9 percent normative corundum. Based on Urabe's results, this melt has good potential to generate magmatic aqueous fluids with high concentrations of metals.

Creasey (1984) compared the geochemistry of mineralized (Schultze Granite) and barren (Tea Cup Granodiorite and Granite Basin Porphyry) Laramide stocks. Ratios of major element cations showed a distinct division between mineralized and unmineralized stocks. Specifically, stocks with Si/(Si + Ca + Mg + Fetotal) ratios higher than 0.91 and K/(K + Ca + Mg + Fetotal) higher than 0.36 were associated with mineralization, whereas all barren stocks had lower ratios. Melt inclusions from the 1977 to 1989 samples have ratios that fall into the barren category. However, the cation ratios of glass in the unhomogenized melt inclusions from the 1991 sample have ratios that are in the range for mineralized rocks. Assuming again that the 1991 glass represents the composition that the melt in the magma chamber will evolve to with continued crystallization, the future White Island melt will have a composition consistent with that observed in mineralized stocks.

Lang and Titley (1998) studied the geochemical and isotopic characteristics of a large number of Laramide magmatic systems in the southwestern United States. These workers noted that productive intrusions show positive europium anomalies, whereas barren intrusions show negative Eu anomalies. Melt inclusions from White Island show positive Eu anomalies (Fig. 9), again suggesting that the magma beneath White Island has potential for generating porphyry copper mineralization in the future. Data for $(Na_2O + K_2O)$ vs. SiO_2 from White Island also plot within the area characteristic of productive intrusions, according to Lang and Titley (1998). Although most of the geochemical signatures of melt inclusions from White Island are consistent with those for mineralized intrusions as reported by Lang and Titley (1998), the Y-Mn (Fig. 11) and high field strength element (HFSE)-Y (Fig. 12) systematics of the melt inclusions at White Island are more characteristic of barren intrusions.

Candela (1989) and Cline and Bodnar (1991) have documented the importance of the initial Cl/H_2O ratio of the melt in terms of the ability of the magmatic aqueous fluid to extract metal from the crystallizing melt. The Cl/H_2O ratio for melt inclusions at White Island is about 0.15, which is beyond the range of data in either of the studies listed above. However, both studies note that the higher the Cl/H_2O ratio, the more efficient the aqueous phase is in removing copper from the melt. (It should be noted, however, that the elevated Cl/H_2O ratio at White Island mostly reflects the low water contents of the melts rather than an elevated Cl content.) Using Cl/H_2O data from White Island and data extrapolated from figure 6 in Cline and Bodnar (1991), only about 5 km^3 of White Island melt would be needed to produce a copper deposit containing 250 Mt of 0.75 percent copper ore. For comparison, the size of the causative intrusion at the Yerington, Nevada, porphyry copper deposit is about 65 km^3 (Dilles, 1987). Thus, it appears that the Cl/H_2O ratio of White Island melts is sufficiently high to cause efficient extraction of copper from the melt into the magmatic aqueous phase. It should also be noted that pyrrhotite, amphibole, biotite, or other phases that

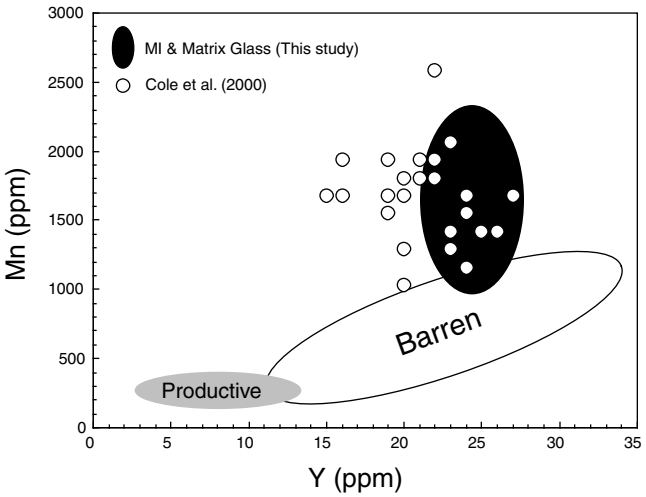

FIG. 11. Mn-Y systematics in melt inclusions and matrix glass from White Island from this study. Also shown are whole-rock values from Cole et al. (2000) and fields for productive and barren porphyry copper intrusions from Lang and Titley (1998).

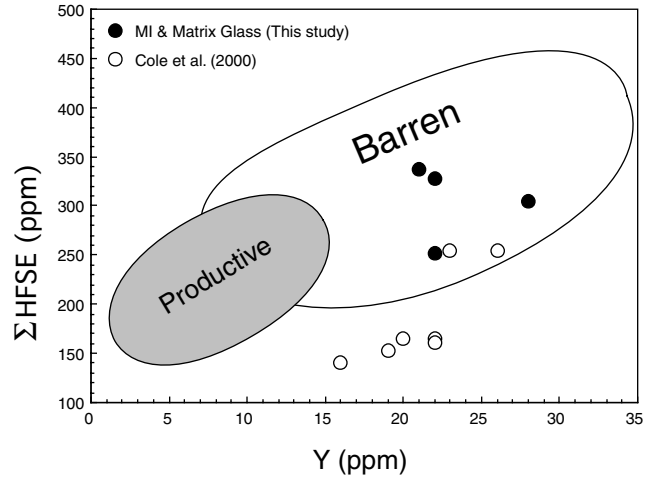

FIG. 12. High field strength elements (HFSE)-Y systematics in melt inclusions and matrix glass from White Island from this study. Also shown are whole-rock values from Cole et al. (2000) and fields for productive and barren porphyry copper intrusions from Lang and Titley (1998).

might serve as sinks for copper (Candela, 1989) have not been recognized during petrographic analysis of ejecta.

Melt inclusions indicate that the sulfur content of the White Island melt may be lower than that of a typical andesitic melt. Additionally, the presence of SO_2 rather than H_2S in the volcanic gas indicates relatively elevated f_{O_2} conditions in the magma chamber (Burnham and Ohmoto, 1980). At magmatic temperatures pyrrhotite is not stable at these f_{O_2} conditions (Whitney, 1980). The low sulfur content and elevated f_{O_2} result in iron being removed from the melt as magnetite rather than as a sulfide phase. This suggests that copper will not be incorporated into solid phases and that the copper concentration in the melt will increase as fractional crystallization continues. Moreover, because White Island is a quiescently discharging arc volcano, Cu is being lost from the magmatic-hydrothermal system to the atmosphere at a much lower rate than would be expected for an explosive arc volcano (Hedenquist, 1995).

Houghton and Nairn (1989b) have constructed a cross section of White Island based on seismic, chemical, and structural data and estimate that the main portion of the magma chamber occurs at a depth of ~3 to 4 km beneath White Island. With an average density of 2.4 to 2.8 g/cm^3 for andesitic liquids and 2.4 to 2.9 g/cm^3 for crust adjacent to andesitic volcanoes (Gill, 1981) the pressure in the magma chamber at that depth would be 720 to 1,160 bars. Candela and Piccoli (1995) reported that the maximum efficiency for partitioning of copper into the magmatic aqueous phase occurs at a pressure of 1 kbar. The efficiency decreases at pressures above and below this value. Thus, the pressure in the deeper magma chamber at White Island appears to be ideal for extraction of copper from the melt into the magmatic fluid. Note that the melt inclusions studied here contain less than 1 wt percent water. The minimum pressure required to dissolve this amount of water in a rhyolitic melt is less than 100 bars (Newman and Lowenstern, 2002).Wardell et al. (2000) found similar low water contents in their melt inclusions and interpreted this to indicate that the melt inclusions were formed at pressures of 35 to 70 bars. An alternative interpretation that we prefer is that the melt inclusions were trapped at higher pressures and deeper in the magma chamber, and the melt was not saturated in water. The absence of fluid inclusions in the White Island samples is consistent with the melt inclusions being trapped in a volatile-undersaturated magma chamber.

The tectonic environment, near-surface gas and water chemistry, and melt chemistry (as evidenced by melt inclusions) at White Island all show features that are characteristic of metal-rich hydrothermal systems and economic porphyry copper deposits. These observations suggest that as the White Island magmatic-hydrothermal system cools and crystallizes during the next 20,000 to 30,000 yr, conditions are likely to be appropriate for generation of porphyry-style mineralization. Moreover, studies of other active magmatic-hydrothermal systems in similar tectonic environments are likely to significantly advance our understanding of the porphyry copper ore-forming process, in a manner similar to the way in which studies of active terrestrial geothermal systems greatly improved our understanding of epithermal ore genesis (Henley and Ellis, 1983; Henley and Hedenquist, 1986).

Acknowledgments

The authors would like to thank J. J. Student for discussions concerning analysis of melt inclusions during the course of this study.We thank Todd Solberg for assistance with electron microprobe analysis and Erik Hauri for guidance during ion probe analysis of melt inclusions. Detailed thoughtful reviews by Hiroshi Shinohara and Jake Lowenstern of an earlier version of this manuscript significantly improved the presentation. The authors accept responsibility for any shortcomings that remain. Partial funding for this work was provided by grant EAR-9527034 from the National Science Foundation to RJB.

REFERENCES

Anders, E., and Grevasse, N., 1989, Abundances of the elements: Meteoric and solar: Geochimica et Cosmochimica Acta, v. 53, p. 197–214.

Anderson, A.T., Jr., 1983, Oscillatory zoning of plagioclase: Nomarski interference contrast microscopy of etched polished sections: American Mineralogist, v. 68, p. 125–129.

Arribas, A., Hedenquist, J.W., Itaya, T., Okada, T., Concepción, R.A., and Garcia, J.S., 1995, Contemporaneous formation of adjacent porphyry and epithermal Cu-Au deposits over 300 ka in northern Luzon, Philippines: Geology, v. 23, p. 337–340.

Audétat, A., Günther, D., and Heinrich, C.A., 2000, Magmatic-hydrothermal evolution in a fractionating granite: A microchemical study of the Sn-W-F mineralized Mole Granite (Australia): Geochimica et Cosmochimica Acta, v. 64, p. 3373–3393.

Beane, R.E., 1982, Hydrothermal alteration in silicate rocks, *in* Titley, S.R., ed., Advances in geology of the porphyry copper deposits of southwestern North America: Tucson, University of Arizona Press, p. 117–137.

Beane, R.E., and Bodnar, R.J., 1995, Hydrothermal fluids and hydrothermal alteration in porphyry copper deposits: Arizona Geological Society Digest 20, p. 83–93.

Beane, R.E., and Titley, S.R., 1981, Porphyry copper deposits.Part II.Hydrothermal alteration and mineralization: Economic Geology 75th Anniversary Volume, p. 235–263.

Black, P.M., 1970, Observations on White Island volcano, New Zealand: Bulletin of Volcanology, v. 34, p. 158–167.

Bodnar, R.J., 1982, Fluid inclusions in porphyry-type deposits, *in* Mineral deposits research review for industry course notes: University Park, Pennsylvania State University, p. RB1–25.

——1995, Fluid-inclusion evidence for a magmatic source for metals in porphyry copper deposits: Mineralogical Association of Canada Short Course, v. 23, p. 139–152.

——1999, Hydrothermal solutions, *in* Marshall, C.P., and Fairbridge, eds., Encyclopedia of geochemistry: Lancaster, Kluwer Academic Publishers, p. 333–337.

Bodnar, R.J., and Beane, R.E., 1980, Temporal and spatial variations in hydrothermal fluid characteristics during vein filling in preore cover overlying deeply buried porphyry copper type mineralization at Red Mountain, Arizona: Economic Geology, v. 75, p. 876–893.

Burnham, C.W., 1979, Magmas and hydrothermal fluids, *in* Barnes, H.L., ed., Geochemistry of hydrothermal ore deposits, 2nd ed.: New York, J. Wiley and Sons, p. 71–136.

——1997, Magmas and hydrothermal fluids, *in* Barnes, H.L., ed., Geochemistry of hydrothermal ore deposits, 3rd ed.: New York, J. Wiley and Sons, p. 63–123.

Burnham, C.W., and Ohmoto, H., 1980, Late-stage processes of felsic magmatism: Mining Geology, v. 8, p. 1–11.

Candela, P.A., 1989, Magmatic ore-forming fluids: Thermodynamic and mass transfer calculations of metal concentrations: Reviews in Economic Geology, v. 4, p. 223–233.
Candela, P.A., and Piccoli, P.M., 1995, Model ore-metal partitioning from melts into vapor and vapor/brine mixtures: Mineralogical Association of Canada Short Course, v. 23, p. 101–127.
Clark, A.H., 1993, Are outsize porphyry copper deposits either anatomically or environmentally distinctive?: Society of Economic Geologists Special Publication 2, p. 213–284.
Clark, R.H., and Cole, J.W., 1989, Volcanic monitoring and surveillance at White Island before the 1976-82 eruption sequence: New Zealand Geological Survey Bulletin, v. 103, p. 9–11.
Cline, J.S., and Bodnar, R.J., 1991, Can economic porphyry copper mineralization be generated by a typical calc-alkaline melt?: Journal of Geophysical Research, v. 96, p. 8113–8126.
Cole, J.W., and Lewis, K.B., 1981, Evolution of the Taupo-Hikurangi subduction system: Tectonophysics, v. 72, p. 1–21.
Cole, J.W., and Nairn, I.A., 1975, Catalogue of the active volcanoes of the world including Solfatara fields. Part 22: New Zealand: International Association of Volcanology and Chemistry of the Earth's Interior, Naples, 156 p.
Cole, J.W., Thordarson, T., and Burt, R.M., 2000, Magma origin and evolution of White Island (Whakaari) volcano, Bay of Plenty, New Zealand: Journal of Petrology, v. 41, p. 867–895.
Creasey, S.C., 1984, The Schultze Granite, the Tea Cup Granodiorite, and the Granite Basin Porphyry: A geochemical comparison of mineralized and unmineralized stocks in southern Arizona: U.S. Geological Survey Professional Paper 1303, 41 p.
Dickinson, W.R., and Hatherton, T., 1967, Andesitic volcanism and seismicity around the Pacific: Science, v. 157, p. 801–803.
Dilles, J.H., 1987, Petrology of the Yerington batholith, Nevada: Evidence for evolution of porphyry copper ore fluids: Economic Geology, v. 82, p. 1750–1789.
Feiss, P.G., 1978, Magmatic sources of copper in porphyry copper deposits: Economic Geology, v. 73, p. 397–404.
Flynn, R.T., and Burnham, C.W., 1978, An experimental determination of rare earth partition coefficients between a chloride containing vapor phase and silicate melts: Geochimica et Cosmochimica Acta, v. 42, p. 685–701.
Giggenbach, W.F., 1987, Redox processes governing the chemistry of fumarolic gas discharges from White Island, New Zealand: Applied Geochemistry, v. 2, p. 143–161.
Giggenbach, W.F., and Glasby, C., 1977, The influence of thermal activity on the trace metal distribution in marine sediments around White Island, New Zealand: New Zealand Department of Science and Industry Research Bulletin, v. 218, p. 121–126.
Giggenbach, W.F., and Sheppard, D.S., 1989, Variations in the temperature and chemistry of White Island fumarole discharges 1972–85: New Zealand Geological Survey Bulletin, v. 103, p. 119–126.
Giggenbach, W.F., Shinohara, H., Kusakabe, M., and Ohba, T., 2003, Formation of acid volcanic brines through interaction of magmatic gases, seawater, and rock within the White Island volcanic hydrothermal system, New Zealand: Society of Economic Geologists Special Publication 10, p. 19–40.
Gill, J.B., 1981, Orogenic andesites and plate tectonics: Berlin, Springer Verlag, 390 p.
Hamilton, R.M., and Gale, A.W., 1968, Seismicity and structure of North Island, New Zealand: Journal of Geophysical Research, v. 73, p. 3859–3876.
Hauri, E., Wang, J., Dixon, J.E., King, P.L., Mandeville, C., and Newman, S., 2002, SIMS analysis of volatiles in silicate glasses 1. Calibration, matrix effects and comparisons with FTIR: Chemical Geology, v. 183, p. 99–114.
Hedenquist, J.W., 1995, The ascent of magmatic fluid: Discharge versus mineralization: Mineralogical Association of Canada Short Course, v. 23, p. 263–289.
Hedenquist, J.W., and Lowenstern, J.B., 1994, The role of magmas in the formation of hydrothermal ore deposits: Nature, v. 370, p. 519–526.
Hedenquist, J.W., Simmons, S.F., Giggenbach, W.F., and Eldridge, C.S., 1993, White Island, New Zealand, volcanic-hydrothermal system represents the geochemical environment of high-sulfidation Cu and Au ore deposition: Geology, v. 21, p. 731–734.
Hedenquist, J.W., Arribas, A., Jr., and Reynolds, T.J., 1998, Evolution of an intrusion-centered hydrothermal system: Far Southeast-Lapanto porphyry and epithermal Cu-Au deposits, Philippines: Economic Geology, v. 93, p. 373–404.
Heinrich, C.A., Ryan, C.G., Mernagh, T.P., and Eadington, P.J., 1992, Segregation of ore metals between magmatic brine and vapor: A fluid inclusion study using PIXE microanalysis: Economic Geology, v. 87, p. 1566–1583.
Heinrich, C.A., Günther, D., Audétat, A., Ulrich,T., and Frischnecht, R., 1999, Metal fractionation between magmatic brine and vapor, determined by microanalysis of fluid inclusions: Geology, v. 27, p. 755–758.
Henley, R.W., and Ellis, A.J., 1983, Geothermal systems ancient and modern: A geochemical review: Earth Science Reviews, v. 19, p. 1–50.
Henley, R.W., and Hedenquist, J.W., 1986, Introduction to the geochemistry of active and fossil geothermal systems:, Monograph Series on Mineral Deposits 26, p. 1–22.
Houghton, B.F., and Nairn, I.A., 1989a, The phreatomagmatic and Strombolian eruption events at White Island volcano 1976-82: eruption narrative: New Zealand Geological Survey Bulletin, v. 103, p. 13–23.
——1989b, A model for the 1976-82 phreatomagmatic and strombolian eruption sequence at White Island volcano, New Zealand: New Zealand Geological Survey Bulletin, v. 103, p. 127–136.
——1991, The 1976-1982 Strombolian and phreatomagmatic eruptions of White Island, New Zealand: Eruptive and depositional mechanisms at a "wet" volcano: Bulletin of Volcanology, v. 54, p. 25–49.
Isacks, B., Oliver, J., and Sykes, L.R., 1968, Seismology and the new global tectonics: Journal of Geophysical Research, v. 73, p. 5585–5899.
Kilinc, I.A., and Burnham, C.W., 1972, Partitioning of chloride between a silicate melt and coexisting aqueous phase from 2 to 8 kilobars: Economic Geology, v. 67, p. 231–235.
Lang, J.R., and Titley, R.T., 1998, Isotopic and geochemical characteristics of Laramide magmatic systems in Arizona and implications for the genesis of porphyry copper deposits: Economic Geology, 93, p. 138–170.
Le Cloarec, M.F., Allard, P., Ardouin, B., Giggenbach, W.F., and Sheppard, D.S., 1992, Radioactive isotopes and trace elements in gaseous emissions from White Island, New Zealand: Earth and Planetary Science Letters, v. 108, p. 19–28.
Lindgren, W., 1905, The copper deposits of the Clifton-Morenci district, Arizona: U. S. Geological Survey Professional Paper 43, 375 p.
Lowenstern, J.B., 1995, Applications of silicate-melt inclusions to the study of magmatic volatiles: Mineralogical Association of Canada Short Course, v. 23, p. 71–99
Mason, D.R., and Feiss, P.G., 1979, On the relationship between whole-rock chemistry and porphyry copper mineralization: Economic Geology, v. 74, p. 1506–1510.
Morgan, G.B., VI, and London, D., 1996, Optimizing the electron microprobe analysis of hydrous alkali aluminosilicate glasses: American Mineralogist, v. 81, p. 1176–1185.
Morimoto, M., 1988, Nomenclature of pyroxenes: Mineralogical Magazine, v. 52, p. 535–550.
Newman, S., and Lowenstern, J.B., 2002, VOLATILEVALC: A silicate melt-H_2O-CO_2 solution model written in Visual basic for excel: Computers and Geosciences, v. 28, p. 597–604.
Norton, D., 1982, Fluid and heat transport phenomena typical of copper-bearing pluton environments: southwestern Arizona, *in* Titley, S.R. ed., Advances in geology of the porphyry copper deposits of southwestern North America: Tucson, University of Arizona Press, p. 59–72.
Pouchou, J.L., and Pichoir, F., 1985, "PAP" Procedure for improved quantitative microanalysis: Microbeam Analysis, v. 20, p. 104–105.
Rapien, M.H., 1998, Geochemical evolution at White Island, New Zealand: Unpublished M.S. thesis, Blacksburg, Virginia Polytechnic Institute and Stage University, 59 p.
Reed, M.J., Candela, P.A., and Piccoli, P.M., 2000, The distribution of rare earth elements between monzogranitic melt and the aqueous volatile phase in experimental investigations at 800°C and 200 MPa: Contributions to Mineralogy and Petrology, v. 140, p. 251–262.
Roedder, E., 1979, Origin and significance of magmatic inclusions: Bulletin de Mineralogie, v. 102, p. 487–510.
Roedder, E., and Bodnar, R.J., 1997, Fluid inclusion studies of hydrothermal ore deposits, *in* Barnes, H.L., ed., Geochemistry of hydrothermal ore deposits, 3rd ed.: New York, Wiley and Sons, p. 657–698.

Rose, W.I., Chuan, R.L., Giggenbach, W.F., Kyle, P.R., and Symonds, R.B., 1986, Rates of sulfur dioxide and particle emissions from White Island Volcano, New Zealand, and an estimate of the total flux of major gaseous species: Bulletin of Volcanology, v. 48, p. 181–188.

Sales, R.H., 1954, Genetic relations between granites, porphyries and associated copper deposits: Mining Engineering, v. 6, p. 499–505.

Sawkins, F.J., 1984, Metal deposits in relation to plate tectonics: Berlin, Springer-Verlag, 325 p.

Shinohara, H., 1994, Exsolution of immiscible vapor and liquid from a crystallizing silicate melt: Implications for chlorine and metal transport: Geochimica et Cosmochimica Acta, v. 58, p. 5215–5221.

Shinohara, H., and Hedenquist, J.W., 1997, Constraints on magma degassing beneath the Far Southeast porphyry Cu-Au deposit, Philippines: Journal of Petrology, v. 38, p. 1741–1752.

Sillitoe, R.H., 1972, A plate tectonic model for the origin of porphyry copper deposits: Economic Geology, v. 67, p. 184–197.

——1983, Enargite-bearing massive sulfide deposits high in porphyry copper systems: Economic Geology, v. 78, p. 348–352.

——1995, The influence of magmatic-hydrothermal models on exploration strategies for volcano-plutonic arcs: Mineralogical Association of Canada Short Course, v. 23, p. 511–525.

Sobolev, A.V., Kamenetskiy, V.S., Metrich, N., Clocchiatti, R., Kononkova, N.N., DeVirts, A.L., and Ustinov, V.I., 1990, Volatile regime and crystallization conditions in Etna hawaiite lavas: Geochemistry International, v. 1991, p. 53–65.

Stringham, B., 1960, Differences between barren and productive intrusive porphyry: Economic Geology, v. 55, p. 1622–1630.

Student, J.J., 2002, Silicate melt inclusions in igneous petrogenesis: Unpublished Ph.D. dissertation, Blacksburg, Virginia Polytechnic Institute and Stage University.

Tedesco, D., and Toutain, J.P., 1991. Chemistry and emission rate of volatiles from White Island Volcano (New Zealand): Geophysics Research Letters., v. 8, p. 113–116.

Titley, S.R., and Beane, R.E., 1981, Porphyry copper deposits: Part I. Geological settings, petrology, and tectogenesis: Economic Geology 75th Anniversary Volume, p. 214–235.

Urabe, T., 1985, Aluminous granite as a source magma of hydrothermal ore deposits: An experimental study: Economic Geology, v. 80, p. 148–157.

Wardell, L.J., Kyle, P.R., Dunbar, N., and Christenson, B., 2000, White Island volcano, New Zealand: Carbon dioxide and sulfur dioxide emission rates and melt inclusion studies: Chemical Geology, v. 177, p. 187–200.

Whitney, J.A., 1980, Volatiles in magmatic: Reviews in Economic Geology, v. 1, p. 155–175.

Williams T.J., Candela P.A., and Piccoli P.M., 1995, The partitioning of copper between silicate melts and two-phase aqueous fluids: An experimental investigation at 1 kbar, 800°C and 0.5 kbar, 850°C: Contributions to Mineralogy and Petrology, v. 121, p. 388–399.

Wood, C.P., and Browne, P.R.L., 1996, Chlorine-rich pyrometamorphic magma at White Island volcano, New Zealand: Journal of Volcanology and Geothermal Research, v. 72, p. 21–35.